




# Comparative Analysis of Histological Tools for Myelin

Zihui An<sup>1</sup> · Shuo Yan<sup>2</sup> · Jiayi Wang<sup>1</sup> · Hanqing Qiu<sup>1</sup> ·  
Binghua Xie<sup>1</sup> · Shumei Feng<sup>3</sup> · Mengsheng Qiu<sup>1</sup> ·  
Zhou Tan<sup>1</sup> 

Received: 12 December 2024 / Accepted: 24 April 2025

© Center for Excellence in Brain Science and Intelligence Technology, Chinese Academy of Sciences 2025

**Abstract** Myelin is an essential structure that facilitates rapid saltatory conduction in the nervous system. Discrepancies in myelin microstructure are a hallmark of numerous neurological disorders, rendering the assessment of myelin integrity and content an indispensable tool in clinical diagnostics and neuroscience research. Extensive research has been dedicated to scrutinizing its biochemical makeup and morphology under normal, pathological, and experimental conditions over the years. In this review, we present an updated summary of the myelin sheath's structure, composition, and developmental trajectory. We systematically enumerate and contrast eight prevalent myelin staining techniques across dimensions of sensitivity, specificity, and resolution, delving into their underlying staining principles. With an initial application of myelin histology on the mouse demyelination model, our review accentuates the accurate delineation of myelination and the microstructural analysis of the myelin sheath. Such insights are anticipated to significantly contribute to the evaluation and understanding of white matter pathologies.

**Keywords** Myelin · Corpus callosum · White matter · Spinal cord · Demyelination · Histology

## Introduction

Applying silver carbonate staining techniques, pioneers Pio Del Rio Hortega and Wilder Penfield first delineated the intricate morphology of oligodendrocytes (OLs), showcasing that their delicate processes extend to form myelin sheaths [1]. This seminal work revealed the pivotal role of OLs in generating the multilamellar myelin membranes that ensheath axons within the central nervous system (CNS). Subsequent advancements in histochemical [2] and fluorescence-based [3] methodologies have enabled us to discern the nuanced and distinctive myelin architecture under both light and fluorescence microscopy. Given the substantial disparities in cellular origin, developmental trajectories, and pathological manifestations between the myelin sheaths of the peripheral nervous system (PNS), governed by Schwann cells, and those of the CNS [4], this review primarily concentrates on the histology of CNS myelin.

## Structure of Myelin

Histological staining is intended to visualize the myelin structure to track pathological changes. For instance, when stained with Luxol fast blue (LFB), the myelin sheath typically appears as a peripheral ring around the axon in cross-sections and as a long, parallel projection in longitudinal sections. This morphological feature helps elucidate the relationship between the myelin sheath and the axon. Electron microscopy studies of myelin sheaths have vividly depicted the multilayered compaction of the plasma membrane of OLs around axons [5], culminating in the formation of myelinated nerve fibers (Fig. 1A, B). These highly specialized and intricate three-dimensional structures can be effectively represented in two dimensions through cross-sectional and

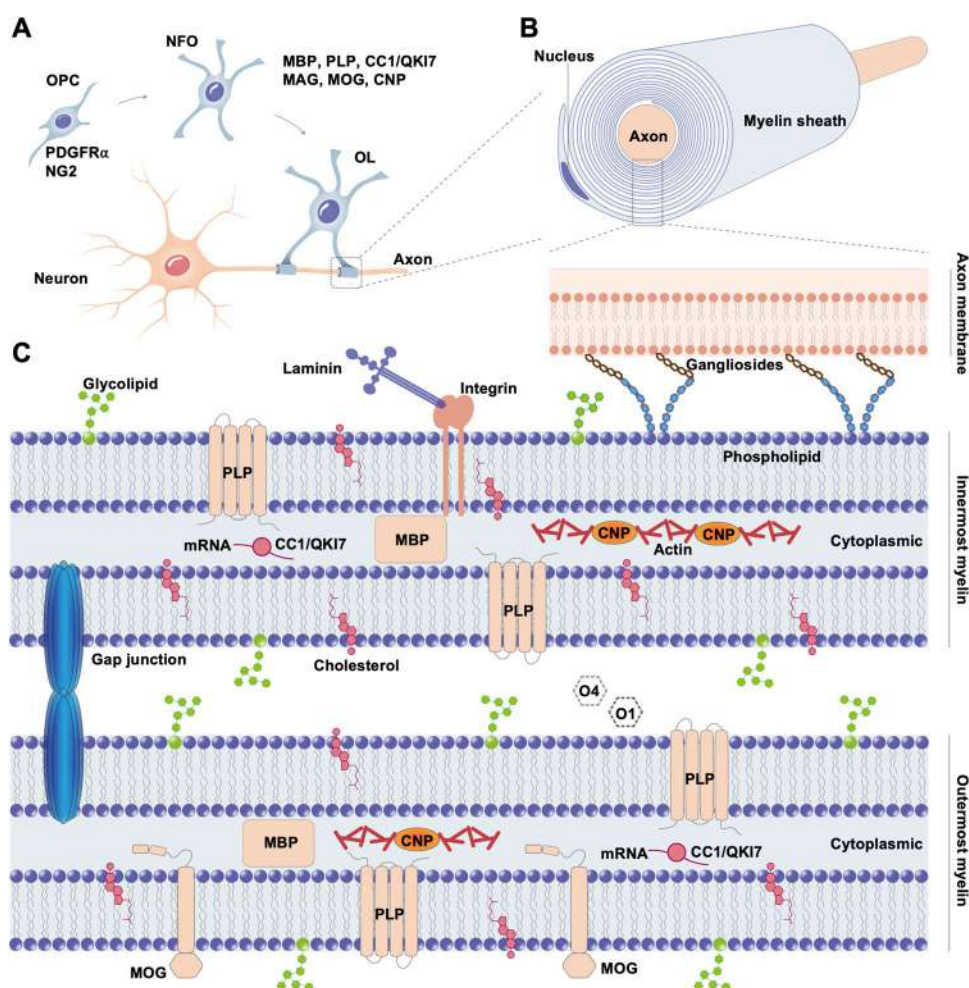
✉ Zhou Tan  
tanzhou@hznu.edu.cn

<sup>1</sup> Zhejiang Key Laboratory of Organ Development and Regeneration, College of Life and Environment Sciences, Hangzhou Normal University, Hangzhou 311121, China

<sup>2</sup> PLA Naval Medical Center, Shanghai 200052, China

<sup>3</sup> Department of Histology and Embryology, School of Basic Medical Sciences, Xinjiang Medical University, Urumqi 830017, China

**Fig. 1** Overview of CNS Myelin Formation and Structure. **A** Developmental trajectory of the oligodendrocyte lineage, highlighting the expression of PDGFR $\alpha$  and NG2 in OPCs. Newly-formed OLs and mature myelinating OLs exhibit the expression of key myelin proteins: MBP, PLP, CC1/QKI7, MAG, MOG, and CNP. **B** Structure of the myelin sheath encircling a nerve fiber, showcasing its multilamellar organization. **C** Schematic representation of the principal myelin components. OPC, oligodendrocyte precursor cell; NFO, newly-formed oligodendrocyte; OL, oligodendrocyte; PDGFR $\alpha$ , platelet-derived growth factor receptor  $\alpha$ ; NG2, also referred to as CSPG4, chondroitin sulfate proteoglycan 4; MBP, myelin basic protein; PLP, proteolipid protein; MAG, myelin-associated glycoprotein; MOG, myelin oligodendrocyte glycoprotein; CNP, 2',3'-cyclic nucleotide 3'-phosphodiesterase.



longitudinal views. In cross-sectional examination, the multilamellar membrane of OLs encircling the axon is characterized by alternating electron-dense and electron-lucent layers, corresponding to the major dense line (reflecting the residual intracellular space) and the intraperiod line (representing the extracellular space between adjacent spiral layers), with a periodic separation of  $\sim 12$  nm [6, 7]. Conversely, longitudinal sections of the myelin sheath delineate a typical myelin structure, featuring a nodal region that measures  $\sim 1$   $\mu$ m in width, a paranodal domain  $\sim 4$   $\mu$ m in length, a juxtaparanodal domain that stretches 10 to 15  $\mu$ m, and an internode region that may span an impressive 2 mm in length [8, 9].

Functionally, the intercellular junctions within the myelin sheath can be categorized into three distinct types: the radial component [10], the axon-OL junction [11], and the gap junction [12]. These junctions establish anchoring connections between the multilamellar membranes or between the OL and the axon [13]. Specifically, the radial component and the axon-OL junction serve to provide electrical insulation by limiting ionic current leakage across the myelin sheath [14]. In contrast, gap junctions facilitate metabolic transport, spatial buffering, and electrical coupling [15–17]. From a

molecular perspective, the radial component is classified as a tight junction, composed of proteins such as Claudin-11 [18, 19]. The axon-OL junction, on the other hand, is mediated by interactions involving myelin-associated glycoprotein (MAG) and contactin-associated protein (Caspr), which link the myelin sheath to the axon [20]. Gap junctions are primarily formed by the conventional gap junction proteins, the connexins [21], which create intercellular channels that allow for the diffusion of metabolites [22, 23]. Therefore, the structural characteristics of the myelin sheath influence the choice of staining method. For example, specific staining of the Caspr protein is beneficial for identifying the paranodal regions adjacent to the nodes of Ranvier.

## Myelin Composition

In fact, the fundamental composition of myelin in both the PNS and CNS is predominantly lipid-based [24], constituting  $\sim 70\%$  of its dry weight, aligning with the membrane-based structure of the myelin sheath as previously described [25, 26]. As depicted in Fig. 1C, cholesterol, phospholipids,

and glycolipids constitute the primary components, with their ratio being roughly 2:2:1 [27]. The remaining ~30% consists of myelin proteins that serve pivotal functions, including interacting with lipids to stabilize the myelin structure, such as MAG (Fig. 1B) [28], facilitating intercellular communication, exemplified by 2',3'-cyclic nucleotide 3'-phosphodiesterase (CNP) [29], and compacting adjacent lamellae to form the major dense line through myelin basic protein (MBP) and the intraperiod line *via* proteolipid protein (PLP) (Fig. 1C) [30]. Furthermore, a significant proportion of lipids (~20% molar percentage of total lipids) and proteins, including MAG and myelin OL glycoprotein (MOG), within the myelin sheath are glycosylated [31]. These glycans may play a role in molecular adhesion, recognition, and the formation of a protective myelin barrier [32, 33]. Collectively, these components form the molecular foundation of myelin histology. Therefore, while PLP contributes to the structural integrity of the myelin sheath and exhibits a more continuous, filamentous staining pattern, CNP, being involved in metabolic functions, shows a punctate staining pattern due to its specific localization within the sheath.

## Myelin Development

Mammalian CNS myelination is initiated from a predominantly unmyelinated state at birth [34]; OL populations rapidly expand and myelination proceeds extensively thereafter [35]. This process of myelination and myelin remodeling persists through life's various stages [36]. In the rodent embryonic telencephalon, the initial cohort of OL precursor cells (OPCs) emerges from the NKX2.1<sup>+</sup> (NK2 homeobox 1-positive) medial ganglionic eminence and anterior entopeduncular area in the ventral forebrain during embryonic days E12.5 to E14.5. Subsequently, a second wave of OPCs arises from the lateral and caudal ganglionic eminences around E14.5 to E16.5. The third wave originates from dorsal cortical neural progenitors at ~E17.5, marking a ventral-to-dorsal developmental gradient [37]. After generation, OPCs undergo swift proliferation and disperse into adjacent areas [38]. In the mouse spinal cord, OPCs initially arise from OL lineage transcription factor 2-positive ventral neuroepithelial cells within the motor neuron progenitor domain at E12.5, followed by generation from ASCL1<sup>+</sup> neuroepithelial domains in the dorsal spinal cord around E14.5 [39]. Differentiation into newly-formed OLs commences at E18 in the spinal cord and between postnatal days P2 and P3 in the forebrain [40]. These newly-formed OLs initiate contact with neuronal axons, express myelin-specific proteins (such as MBP and ASPA), and mature into fully-functional OLs, elaborating compact myelin sheaths from P7 (Fig. 1A) [41]. This maturation process is relatively slow, typically

taking 18–21 days for axons to become fully myelinated. Even after reaching maturity, the rate of myelin addition decreases but continues into adulthood. Consequently, immunohistochemistry (IHC) or immunofluorescence (IF) staining for myelin-specific proteins can be applied to visualize the spatial and temporal patterns of myelination during development. For example, the detection of the transcription factor Myelin Regulatory Factor in the forebrain indicates the initiation of newly-formed OL formation, suggesting that the mice are likely at P2.

## Myelin-related Diseases

Dysregulation of myelination underlies a spectrum of neurological disorders, broadly classified into inherited and acquired myelinopathies [42]. As our understanding of myelin deepens, the investigation of myelin-related disorders has expanded, encompassing both prevalent conditions such as multiple sclerosis (MS) and less common genetic anomalies [43, 44]. The myelinopathies constitute a diverse and extensive group characterized by varied clinical presentations, underlying pathophysiological mechanisms, and etiological factors [45]. Nonetheless, establishing a definitive diagnosis of myelin pathology and demyelination within the CNS is contingent upon obtaining clear morphological evidence, which can be challenging to procure. This underscores the importance of meticulously evaluating myelin alterations. For instance, IHC for MBP during critical periods of brain development can reveal how disruptions in these stages may result in long-term neurological deficits. Similarly, in patients with MS, LFB staining demonstrates plaques of demyelination in the brain and spinal cord, which are hallmark pathological features of the disease.

In summary, the complex and delicate structure of the myelin sheath, the variable state of OL development, and diverse application requirements have established higher requirements for the development and selection of appropriate myelin staining methods. Therefore, in this review, we compare and discuss in detail the current major methods of histological staining of myelin and OLs, in order to provide a methodological basis for the study of OL development and myelin structure.

## Comparative Analysis of Myelin Staining

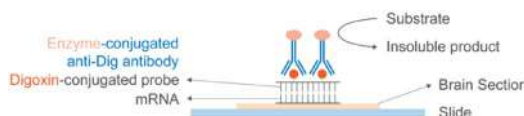
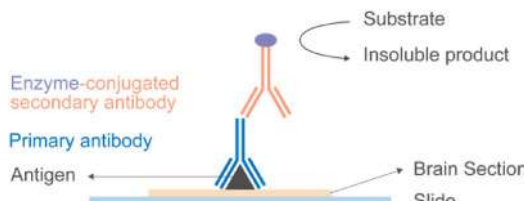
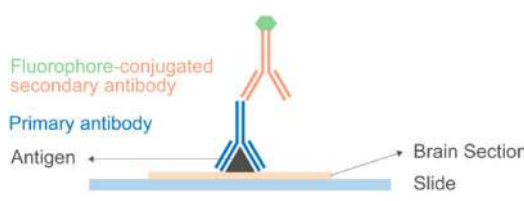

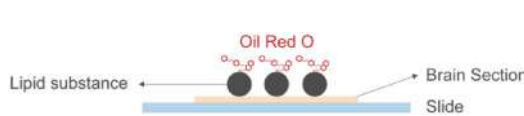
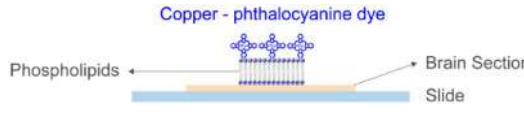
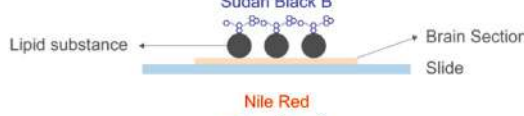

### Principles of Myelin Staining

Analysis indicates that the sensitivity and specificity of myelin staining are intricately linked to the underlying staining principles. Accordingly, we present a comprehensive overview of the potential staining mechanisms for the

eight myelin staining methods in Table 1, along with a comparative assessment of their respective strengths and weaknesses. *In situ*, RNA hybridization (ISH) primarily hinges on the specific expression patterns of myelin-related genes, such as MBP. It indirectly visualizes the myelin sheath by binding *in situ* to myelin gene mRNA, effectively staining OLs rather than directly highlighting the myelin structure itself. IHC and IF offer the advantage of directly staining myelin components using antibodies specific to myelin proteins, which are known for their exceptional sensitivity and specificity. However, their staining resolution is marginally less than that of Gold salt staining, a limitation imposed by the constraints on the chromogenic accuracy of horse-radish peroxidase (HRP) and fluorescence. The underlying

principle of myelin gold salt staining remains a subject of limited in-depth research. It has been documented that gold chloride can delineate myelin structure by interacting with myelin-specific proteins [46]. Given the glycosylation status of some myelin-specific proteins like MAG/MOG and the potential redox reactions between gold salts and sugars, the high degree of concordance between the outcomes of Gold salt and IHC or IF staining lends support to this hypothesis. Furthermore, the uniform staining outcomes observed with the four methods, Oil Red O, LFB, Sudan Black, and Nile Red, implicate a common staining substrate, presumably lipids. It is noteworthy that numerous publications have reported LFB's capacity to stain Nissl bodies and mast cells purple, in addition to staining myelin sheaths blue,

**Table 1** Summary of principles, advantages, and disadvantages of histological techniques

Method	Principle	Advantages	Disadvantages
ISH		Strong specificity High sensitivity	Long experimental period Tedious steps High cost Reliance on high-quality probes and antibodies
IHC		Strong specificity High sensitivity	Long experimental period Tedious steps High cost Reliance on high-quality antibodies Not easy to preserve
IF		Strong specificity High sensitivity	Long experimental period Tedious steps High cost Reliance on high-quality antibodies Not easy to preserve Result invisible to the naked eye
Gold salts		Strong specificity High sensitivity Low cost Simple and quick Easy to preserve	Staining time must be strictly controlled
Oil Red O		Low cost Simple and quick Easy to preserve	Poor specificity Low sensitivity
LFB		Low cost Simple and quick Easy to preserve	Poor specificity Low sensitivity
Sudan Black B		Low cost Simple and quick Easy to preserve	Poor specificity Low sensitivity
Nile Red		Low cost Simple and quick	Poor specificity Low sensitivity Not easy to preserve Result invisible to the naked eye

ISH, *In situ* RNA Hybridization; IHC, Immunohistochemistry; IF, Immunofluorescence; LFB, Luxol Fast Blue.

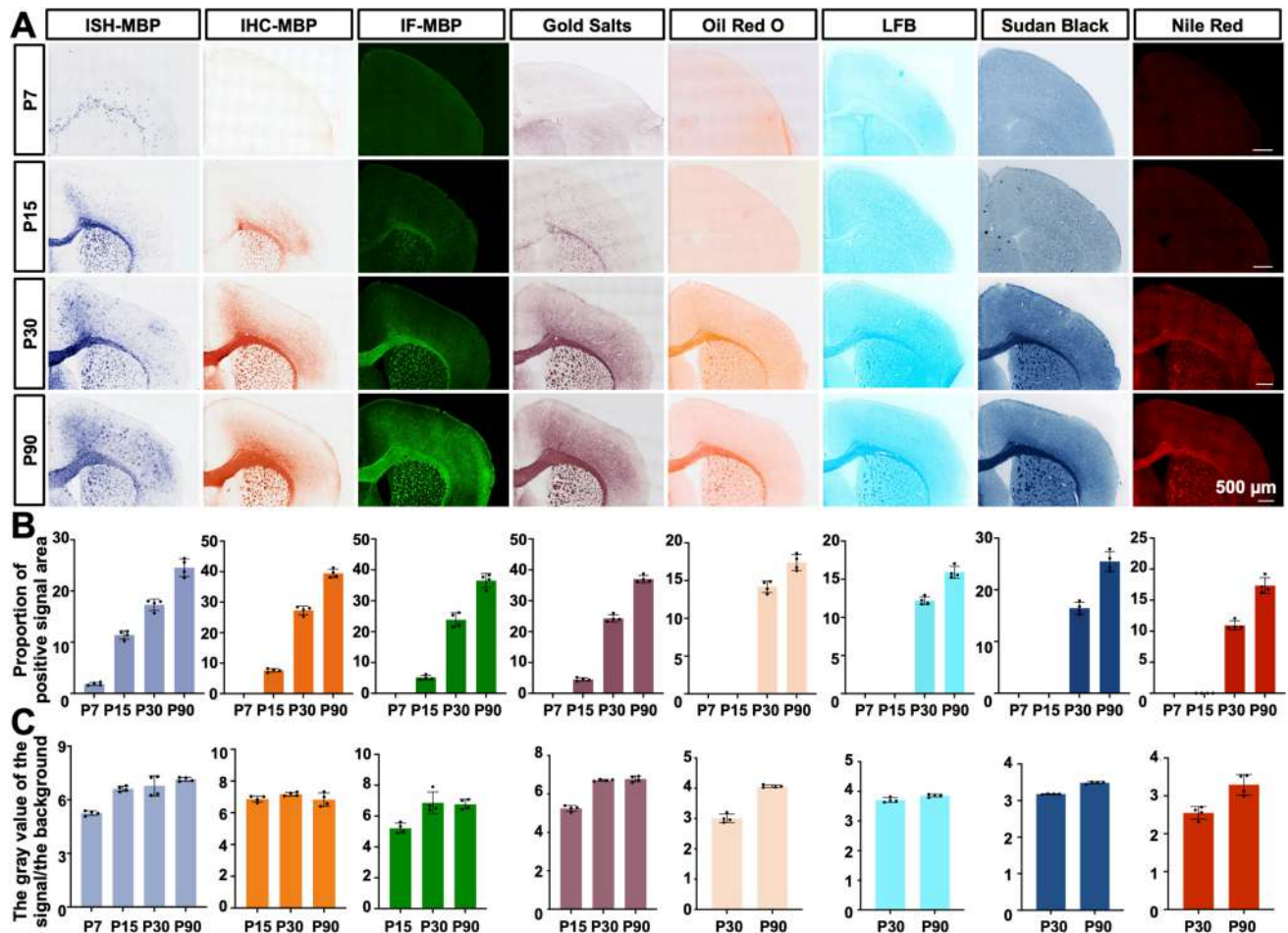


suggesting a staining mechanism that may diverge slightly from the other three methods.

### Myelin Staining in the Brain

As previously indicated, the process of myelination in the cerebral neurons of mice commences on P7 (Fig. 1A), gradually progressing to completion over the ensuing months. By P15, the pace of myelination accelerates, reaching its zenith by P30. Subsequently, the rate of myelination begins to decelerate, culminating in near completion around P90 day [47]. In light of these developmental milestones, we selected these specific time points for the comparative histological analysis of myelin (Fig. 2A), and the statistical results (Fig. 2B) show that among the eight histological methods evaluated, only ISH was able to accurately capture the initiation of myelination signals, whereas the remaining seven methods predominantly

exhibited either no signal or merely background noise. At the peak acceleration of myelination on P15, four methods (ISH, IHC, IF, and Gold salt staining) demonstrated robust myelin staining signals (signal-to-noise ratio > 5), notably in the corpus callosum region (Fig. 2B, C). In contrast, Oil Red O, LFB, Sudan Black, and Nile Red staining failed to detect myelin signals. Upon reaching the peak of myelination at P30, all eight methods yielded valid myelin staining signals. Compared to the findings at P15, the initial four staining methods (ISH, IHC, IF, and Gold salt staining) exhibited enhanced staining efficacy, characterized by intensified signal intensity and broadened areas of staining. Ultimately, the enhancement in staining signal can be observed in all of the methods at P90, and the expansion of the myelinated area persists, indicating that myelination retains a gradual growth trajectory even at this advanced stage.



**Fig. 2** Application of Histological Staining Methods to the Developing Mouse Brain. **A** Overview of the outcomes from eight distinct histological staining techniques applied across four critical developmental stages of the mouse brain (postnatal days P7, P15, P30, and P90). Scale bars, 500  $\mu$ m. **B** Statistical analysis of the myelin staining

area in **A** ( $n=4$ ). **C** Statistical analysis of the signal-to-noise ratio of the myelin staining in **A** ( $n=4$ ). Abbreviations: ISH, *In Situ* Hybridization; IHC, Immunohistochemistry; IF, Immunofluorescence; LFB, Luxol Fast Blue.

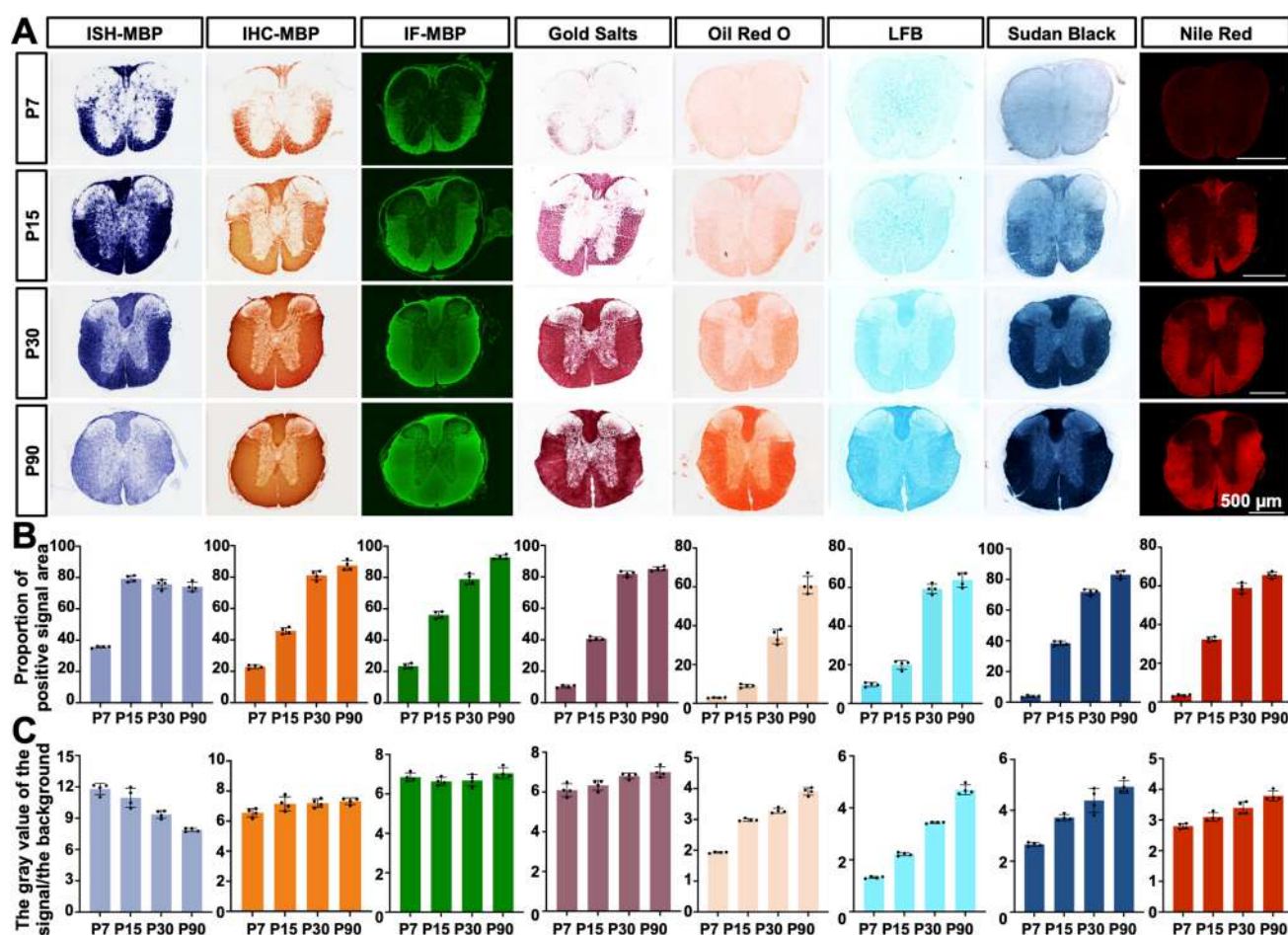
## Myelin Staining in the Spinal Cord

In contrast to cerebral myelination, spinal cord myelination in mice is characterized by a more rapid developmental trajectory. Myelination in the spinal cord is initiated on the day of birth (P0), showing a surge in the rate of myelination by P7, reaching a peak by P15, and nearing completion by P30 [34, 48]. As depicted in Fig. 3A and B, the initial four staining methods (ISH, IHC, IF, and Gold salt staining) demonstrate discernible positive staining signals at the rapidly myelinating stage of P7, whereas the latter four methods only reveal background signals (Fig. 3C). From the onset of the myelination peak through to the completion phase at P15–P30, all eight methods yield positive staining signals. Compared with the P7 stage, these methods also exhibit an increase in staining intensity and expansion of the stained area, indicative of a dose effect. In alignment with the cerebral findings, even at P90, the spinal cord myelination maintains a continued, albeit slow,

growth, suggesting a persistent, low-rate progression of the myelination process.

## Sensitivity and Resolution of Staining

The comparison of sensitivity and specificity serves as a critical assessment of the various staining methods' capabilities to monitor myelination (Table 2). Fig. 2 clearly illustrates that ISH was the first method to detect signals, suggesting that while myelin-related genes initiate mRNA expression by P7, the synthesis of corresponding proteins, lipids, or polysaccharides, and hence the formation of the myelin structure, may still be in its early phases. From a structural perspective, IHC and IF staining exhibit similar sensitivities, which are marginally superior to that of Gold salt staining (Fig. 3). This enhanced sensitivity might be attributed to the signal amplification afforded by the secondary antibodies. A synthesis of the results shown in Figs 2 and 3 indicates that the Oil Red O,



**Fig. 3** Histological Staining Techniques in the Developing Mouse Spinal Cord. **A** Comprehensive summary of staining outcomes utilizing eight histological methods across the development of the spinal

cord at P7, P15, P30, and P90. Scale bars, 500  $\mu$ m. **B** Statistical analysis of the myelin-stained area in **A** ( $n = 4$ ). **C** Statistical analysis of the signal-to-noise ratio of the myelin staining in **A** ( $n = 4$ ).

**Table 2** Overview of histological staining methods

Method	Staining effect				Cost	
	Color		Specificity	Sensitivity	Time	Money
	Signal	Background				
ISH	Based on the substrate	Almost colorless	+++	+++	3 days	++++
IHC	Based on the substrate	Almost colorless	+++	++	2 days	+++
IF	Based on the fluorophore conjugated on secondary antibody	Almost colorless	+++	++	2 days	+++
Gold salts	Purple	Almost colorless	+++	++	1 h	++
Oil Red O	Orange	Pale orange	++	+	1 h	+
LFB	Brilliant blue	Pale blue	++	+	3 h	+
Sudan Black B	Navy blue	Blue	++	+	1 h	+
Nile Red	Orange-red fluorescence	Pale orange	+	+	0.5 h	+

Specificity: SNR < 3, +; SNR 3-6, ++; SNR > 6, +++. Sensitivity: P30, +; P15, ++; P7, +++. Cost: <\$100, +; \$100-500, ++; \$500-1000, +++; > \$1000, ++++.

This table provides a summary of the staining effectiveness and associated costs for various histological methods. The staining specificity, sensitivity, and monetary cost are indicated by the number of “+” symbols, where a higher number corresponds to greater specificity, heightened sensitivity, and increased cost.

LFB, Sudan Black, and Nile Red stains are markedly less sensitive than the initial four methods. Regarding the resolution of the stained images, the first three methods (ISH, IHC, and IF) displayed pronounced punctate or flaky signals in regions of high signal intensity. Notably, Gold salt staining revealed a remarkably clear filamentous nerve fiber structure, a characteristic that may be linked to the principles of color development inherent in these staining techniques.

### Specificity of Stains

When evaluating the concordance between the staining signals of brain and spinal cord sections and the CNS myelination process, all eight methods demonstrated distinct staining specificity. To streamline comparison, we have compiled a summary of the staining signal, background, sensitivity, specificity, and time/money costs for these methods in Table 2. Upon examination of Figs 2 and 3, it is evident that the latter four methods (Oil Red O, LFB, Sudan Black, and Nile Red) exhibit a higher background signal. Particularly, Oil Red O and LFB display non-specific punctate aggregation signals, potentially attributable to the affinity of Oil Red O for lipid droplets and LFB for Nissl bodies. A detailed discussion of these principles, including their implications for specificity, is provided in the subsequent comparison of staining mechanisms.

### Time/Money Costs

Ultimately, as listed in Table 2, the cost of reagents and the expenditure of time are also pivotal considerations for

the practical application of histological techniques. Among the eight methods we examined, five chemical staining approaches were notably more efficient and economical in terms of reagent use and time. Notably, Nile Red staining stands out as the most expeditious, with the entire staining process achievable within a 1-h timeframe. In contrast, the ISH, IF, and IHC methods incur higher costs due to their requirement for highly specific probes and antibodies. In addition, these methods demand a more extended period, typically ranging from 2 to 3 days, due to their intricate procedural steps.

## Summary of Methods of Histological Assessment of Myelin

### Animals and Tissue Processing

Female C57BL/6 mice at various developmental stages (7, 15, 30, and 90 days old) were procured from the Shanghai Jihui Laboratory Animal Care Co., Ltd (Shanghai, China). The animals were maintained under conditions that adhered to the international standards for laboratory animal care. The protocol (2023121) for the experiment was approved, and animals were handled according to the ethical standards of the Institutional Animal Care and Use Committee of Hangzhou Normal University. To induce demyelination, the mice were fed a diet containing 0.2% cuprizone (w/w), following the protocol detailed in our previous publication [49].

To harvest tissue, each mouse was subjected to transcardiac perfusion with 1× phosphate-buffered saline (PBS) followed by 4% paraformaldehyde (PFA) under avertin-induced



anesthesia. Subsequently, the brain and spinal cord were meticulously dissected, post-fixed in 4% PFA, and dehydrated in a 30% sucrose solution. The tissues were then embedded in an optimal cutting temperature (OCT) compound and cut at 16  $\mu\text{m}$  on a cryomicrotome.

### ***In situ* RNA Hybridization**

ISH was applied as described by Schaeren-Wiemers and Gerfin-Moser [50] with minor modifications [51]. In brief, the digoxigenin-labeled *Mbp* riboprobe corresponding to 1485–2453 of mouse *Mbp* mRNA (accession # NM\_010777.3, NCBI) was used. Images were acquired under a Nikon Eclipse 90i microscope. To prevent RNA degradation, it was essential to wear a mask throughout the experiment and maintain a clean environment to minimize the risk of RNase contamination.

### **Immunohistochemistry**

Endogenous peroxidase activity was quenched by a 10-min incubation at room temperature (RT) in a solution containing a final concentration of 3% hydrogen peroxide in distilled water. Subsequently, slides were thoroughly rinsed in PBS for three cycles of 5 min each. They were then incubated in a blocking solution comprising 5% goat serum and 0.1% Triton X-100 in PBS for 1 h at RT [52]. The blocking solution was then replaced with a primary antibody solution containing rabbit anti-MBP (Abcam, Cambridge, UK) diluted to 1:5000 in 5% goat serum in PBS, and the slides were incubated at 4°C overnight. On the following day, the slides were rinsed again in PBS for three cycles of 5 min each, followed by a 1-h incubation at RT with the secondary antibody, goat anti-rabbit IgG-HRP (Invitrogen, Carlsbad, USA) at a dilution of 1:1000 in the antibody solution. After three final rinses in PBS, the sections were developed to reveal a positive signal for MBP using an HRP chromogenic substrate kit (OasisBiofarm, Hangzhou, China). In the final stage of the experiment, it is crucial to emphasize that both temperature and time play pivotal roles in determining the rate of chromogen development. Meticulous monitoring throughout this phase is imperative to prevent two potential issues: excessive chromogen deposition and heightened background staining. These undesirable outcomes typically occur when either the temperature exceeds optimal levels or the incubation period is extended beyond the recommended duration.

### **Immunofluorescence**

The sections were initially incubated in a blocking solution consisting of 5% goat serum and 0.1% Triton X-100 in PBS for 1 h at RT. This solution was then carefully aspirated,

and the sections were incubated with the primary antibody, rabbit anti-MBP (Abcam), diluted to 1:5000 in a solution of 5% goat serum in PBS, overnight at 4 °C. The following day, the sections were rinsed in PBS for three cycles of 5 min each to remove any unbound primary antibody. Subsequently, they were incubated with the secondary antibody, goat anti-rabbit conjugated to Alexa Fluor 488 (Invitrogen), diluted to 1:3000 in the antibody solution for 1 h at RT. After another series of rinses in PBS, the sections were incubated with 4',6-Diamidino-2-Phenylindole (DAPI; Thermo Fisher Scientific, Waltham, USA) for 5 min to stain the nuclei. The final step involved rinsing the slides in PBS for three cycles of 5 min each to ensure complete removal of any residual reagents. The sections were then prepared for microscopy by coverslipping with a Mowiol mounting medium, which provides a clear and stable visualization of the specimens [53].

### **Gold Salt Staining**

For the gold salt staining, sections were processed using the TrueGold Myelin Staining Kit (OasisBiofarm). In accordance with the manufacturer's instructions, the sections were immersed in 1× TrueGold staining solution, diluted with distilled water, and incubated for 30 min at 45 °C. The staining reaction was then promptly halted by treating the sections with 1× terminating solution for 2 min at RT. Following this, the sections were rinsed twice with PBS for 5 min each to remove any excess reagent. The procedure was concluded by coverslipping the sections with a Mowiol mounting medium, which provided a durable and transparent medium for subsequent microscopic examination [46]. During the experiment, precise control of both the duration and temperature of the staining process, as well as its termination, is crucial. This meticulous regulation helps prevent two potential issues: (1) elevated background staining due to over-staining, which may result in a purple hue, and (2) loss of staining intensity due to excessive termination.

### **Oil Red O Staining**

Tissue sections were evaluated using an Oil Red O Staining Kit (Beyotime, Shanghai, China). Following the manufacturer's protocol, the sections were incubated in the staining solution for 20 min at RT. Then, the stain was briefly rinsed off with wash buffer for 30 s, followed by two thorough rinses in PBS for 5 min each to ensure complete removal of the staining solution. The sections were then prepared for examination by coverslipping with a Mowiol mounting medium, which offers a clear and stable platform for microscopic analysis [54, 55]. The Oil Red O staining solution contained a significant amount of isopropyl alcohol as its



solvent. Therefore, care must be taken during the staining process to prevent evaporation, which may cause the sections to dry out. Similarly, the solvents used in LFB and Sudan Black B staining solutions also contain a high proportion of organic compounds, such as ethanol. As a result, it is equally important to minimize evaporation during these procedures to avoid drying of the sections.

### Luxol Fast Blue Staining

Tissue sections were processed utilizing the LFB Myelin Stain Kit (Solarbio, Beijing, China). In strict accordance with the kit's instructions, the sections were immersed in the LFB staining solution and incubated for 2 h at a controlled temperature of 56 °C. Subsequently, the sections were rinsed in a solution of 95% ethanol, followed by a differentiation solution to meticulously remove any surplus staining. To conclude the staining protocol, the slides underwent three successive rinses in PBS to ensure the removal of all traces of the staining reagents. The sections were then prepared for microscopic examination by coverslipping with a Mowiol mounting medium, which provides a durable and transparent medium for the preservation and visualization of the stained sections [56].

### Sudan Black B Staining

The Sudan Black B staining solution was prepared to a final concentration of 0.3% using absolute ethanol, following the product specifications (Aladdin, Shanghai, China). The sections were immersed in the prepared staining solution and allowed to stain for 30 min at RT. After staining, the sections were rinsed three times in PBS for 5 min each to eliminate any unbound stain. Then, the slides were dehydrated and mounted using a Mowiol mounting medium, which ensures the sections are securely adhered to and protected for long-term storage and high-quality microscopic analysis [57].

### Nile Red Staining

A stock solution of Nile Red (Solarbio) was carefully prepared to achieve a final concentration of 6 mM in Dimethyl Sulfoxide. Subsequently, this stock solution was diluted with PBS to a working concentration of 10 µM to form the staining solution. The sections were then incubated in this staining solution for 10 min at RT, allowing for adequate staining. Following incubation, the sections were thoroughly rinsed in PBS for three cycles of 5 min each to remove any excess stain. The final step involved coverslipping the sections with a Mowiol mounting medium, ensuring the preservation and

clarity of the stained specimens for microscopic examination [58]. In addition, similar to immunofluorescence, prolonged or direct exposure to excitation light should be avoided to prevent photobleaching or photodegradation reactions.

### Statistical Analysis

All images were processed and analyzed using the publicly available ImageJ software (version 2.0.0/1.52p, <https://imagej.net/Fiji/>, accessed on 4 June 2020).

### Specificity Analysis

Images were converted to 8-bit grayscale, and fluorescent images were inverted to ensure a light background and dark positive signals. The threshold was adjusted to match the true intensity of the image. The signal-to-noise ratio (SNR) was calculated as the ratio of the gray value of the positive signal to the gray value of the background. Specificity was categorized based on SNR values: SNR < 3, +; SNR 3–6, ++; SNR > 6, +++.

### Sensitivity Analysis

Images were converted to 8-bit grayscale. The threshold was adjusted to match the true intensity, and fluorescent images were set to a black background. The ImageJ Built-In Automatic Global Threshold Calculation was used to determine the proportion of the area of positive signals relative to the whole brain/spinal cord tissue. Sensitivity was defined based on the earliest detection time of positive signals in brain tissue: P30, +; P15, ++; P7, +++.

### Cost Analysis

Costs were categorized as follows: <\$100, +; \$100–500, ++; \$500–1000, +++; >\$1000, ++++.

### Discussion and Limitations

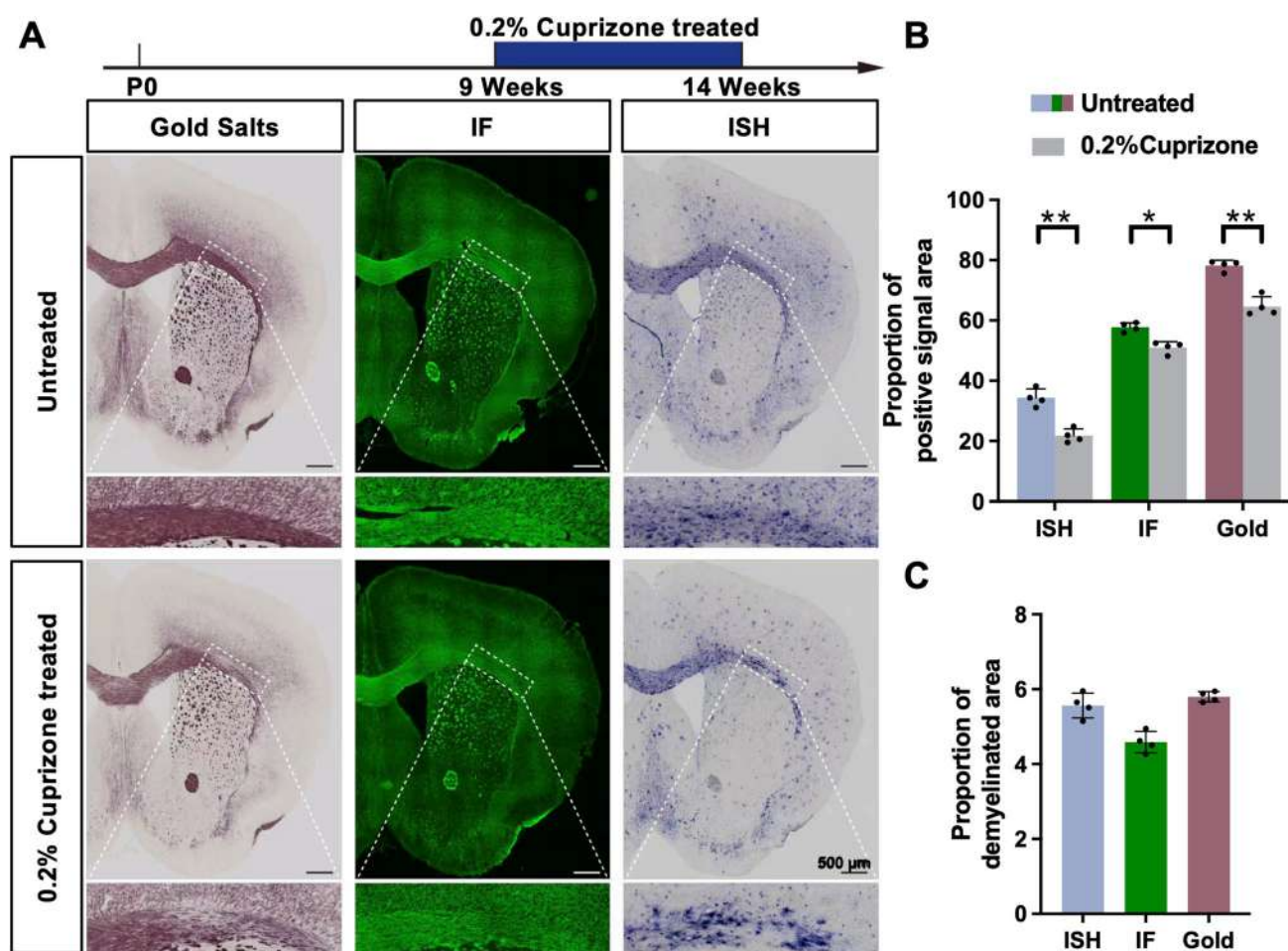
In addition to the qualitative comparative analyses presented, quantitative assessments of myelination staining offer an objective means to gauge the extent of myelination or the severity of demyelination. A variety of quantitative methodologies have been documented for different staining techniques [59]. For instance, the Simple Neurite Tracer, originally a tool for analyzing neuronal protrusions, has been repurposed to quantify the number and length of myelin sheaths visualized through CNP immunofluorescence [60]. Meanwhile, the immunodensity of MBP, as indicated by the mean grey value measured *via* ImageJ software [61],

is determined by subtracting the background staining mean value. Teo et al. have also demonstrated that the spectral shifts in Nile Red-stained myelin can detect minute alterations in the physicochemical properties of myelin [62]. Consequently, the integration of myelin staining with quantitative analysis is poised to become an indispensable tool in neurological research.

Beyond considerations of sensitivity, specificity, and cost, the ultimate objective of histological staining is to facilitate the evaluation of conditions such as demyelination. Gold salt, IF, and ISH staining have all proven to be effective for identifying low-intensity demyelinating lesions in the cuprizone model, with consistent demyelination sites across the three methods (Fig. 4A, B). Notably, ISH and Gold salt staining have exhibited superior sensitivity and SNR in demyelinated tissues (Fig. 4C), a finding that aligns

with their performance in staining during development and suggests their promising potential for clinical applications. Demyelinating diseases encompass a spectrum of etiologies, including immune-mediated, virus-mediated, metabolic, and hereditary myelinopathies. Given the distinct staining mechanisms of different myelin staining methods, the targeted selection of these methods for specific myelin pathologies could yield remarkable insights. For example, in autoimmune demyelination, which often targets proteins like MAG, histopathological analysis might benefit more from IHC, IF, or Gold salt staining.

On the other hand, advances in neural tracing technology have addressed the limitations of traditional tissue staining methods, particularly the inability to observe myelin changes in living specimens in real-time. For instance, using two-photon laser confocal microscopy, researchers



**Fig. 4** Comparative Analysis of Demyelination in the Cuprizone (CPZ) Mouse Model. **A** Gold salt staining reveals the most pronounced demyelination effects in the model. After 5 weeks of CPZ treatment, immunofluorescence staining does not demonstrate satisfactory contrast for visualizing demyelination. In contrast, both Gold salt staining and *In Situ* Hybridization (ISH) methods sensitively identify CPZ-induced myelin loss. Notably, ISH signals appear as dis-

continuous dots, which complicates the precise delineation of demyelination areas. In comparison, Gold salt staining provides a uniform and continuous positive signal, enabling the sensitive and accurate assessment of the specific demyelination range, and even reflects changes in fiber morphology. Scale bars, 500  $\mu$ m. **B** Statistical analysis of the myelin staining area in **A** ( $n = 4$ ,  $*p < 0.01$ ,  $**p < 0.001$ ). **C** Statistical analysis of the demyelination area ( $n = 4$ ).

can monitor dynamic myelin alterations in individual oligodendrocytes in PLP-Enhanced Green Fluorescent Protein transgenic mice. Nevertheless, these cutting-edge technologies are not without their drawbacks, including high technical demands, significant costs, and prolonged experimental timelines. Consequently, the selection of an appropriate methodology should be guided by specific research objectives and available experimental resources. Importantly, integrating multiple techniques, such as combining tracer animals with immunofluorescence, offers a more comprehensive approach and holds great potential for advancing our understanding of myelination processes.

We are well aware that technology is constantly advancing, and our research is limited to the reagents that are more readily available and the methods that are easier to apply, but we do not rule out the possibility that more specific molecular markers [63] or antibodies, and better nucleic acids or fluorescent probes will lead to better SNRs; for example, commercial CNP or PLP antibodies may have a more beautiful tissue staining effect on the myelin sheath in the early (P15) or late (P90) developmental stage. On the other hand, our review also focuses on tissue staining techniques under light or fluorescent microscopy and does not include all histological methods, such as electron or immunoelectron microscopy, which often provides more detailed information about the myelin sheath wrapping axons, which is the basis for the research on the ultrastructure of myelin [64]. Therefore, our review can be used as a reference for methods, and in many cases, a combination of methods may be more convincing in presenting new findings in myelin studies.

## Conclusions

Biological development is intricately linked to the maturation of OLs along white matter pathways, which are vital conduits connecting disparate and adjacent brain regions and play a pivotal role in cognitive processing. Our review indicates that the methodologies presented are adept at detecting myelin and myelinated axons within the CNS. Furthermore, the diverse techniques for myelin identification are capable of specifically pinpointing key constituents of myelin. Given the multifaceted structure, intricate composition, and dynamic nature of myelin, coupled with the heterogeneity of myelinopathies, it is imperative to meticulously select the most appropriate method for myelin sheath staining. This selection should be tailored to align with the specific demands in both clinical and experimental settings.

**Conflict of interest** The authors declare that there are no conflicts of interest.

## References

- Gill AS, Binder DK. Wilder penfield, Pío del río-ortega, and the discovery of oligodendroglia. *Neurosurgery* 2007, 60: 940–948.
- Kriszta G, Nemes B, Sándor Z, Ács P, Komoly S, Berente Z. Investigation of cuprizone-induced demyelination in mGFP-driven conditional transient receptor potential ankyrin 1 (TRPA1) receptor knockout mice. *Cells* 2019, 9: 81.
- Moore CS, Hebb ALO, Robertson GS. Inhibitor of apoptosis protein (IAP) profiling in experimental autoimmune encephalomyelitis (EAE) implicates increased XIAP in T lymphocytes. *J Neuroimmunol* 2008, 193: 94–105.
- Brosius Lutz A, Barres BA. Contrasting the glial response to axon injury in the central and peripheral nervous systems. *Dev Cell* 2014, 28: 7–17.
- Luse SA. Formation of myelin in the central nervous system of mice and rats, as studied with the electron microscope. *J Biophys Biochem Cytol* 1956, 2: 777–784.
- Aggarwal S, Yurlova L, Simons M. Central nervous system myelin: Structure, synthesis and assembly. *Trends Cell Biol* 2011, 21: 585–593.
- Stadelmann C, Timmler S, Barrantes-Freer A, Simons M. Myelin in the central nervous system: Structure, function, and pathology. *Physiol Rev* 2019, 99: 1381–1431.
- Hildebrand C, Remahl S, Persson H, Bjartmar C. Myelinated nerve fibres in the CNS. *Prog Neurobiol* 1993, 40: 319–384.
- Salzer JL, Zalc B. Myelination. *Curr Biol* 2016, 26: R971–R975.
- Peters A. A radial component of central myelin sheaths. *J Biophys Biochem Cytol* 1961, 11: 733–735.
- Mierzwa A, Shroff S, Rosenbluth J. Permeability of the paranodal junction of myelinated nerve fibers. *J Neurosci* 2010, 30: 15962–15968.
- Abrams CK, Scherer SS. Gap junctions in inherited human disorders of the central nervous system. *Biochim Biophys Acta* 2012, 1818: 2030–2047.
- Snaidero N, Möbius W, Czopka T, Hekking LHP, Mathisen C, Verkleij D, *et al.* Myelin membrane wrapping of CNS axons by PI(3, 4, 5)P<sub>3</sub>-dependent polarized growth at the inner tongue. *Cell* 2014, 156: 277–290.
- Devaux J, Gow A. Tight junctions potentiate the insulative properties of small CNS myelinated axons. *J Cell Biol* 2008, 183: 909–921.
- Lundgaard I, Osório MJ, Kress BT, Sanggaard S, Nedergaard M. White matter astrocytes in health and disease. *Neuroscience* 2014, 276: 161–173.
- Fünfschilling U, Supplie LM, Mahad D, Boretius S, Saab AS, Edgar J, *et al.* Glycolytic oligodendrocytes maintain myelin and long-term axonal integrity. *Nature* 2012, 485: 517–521.
- Rash JE. Molecular disruptions of the panglial syncytium block potassium siphoning and axonal saltatory conduction: pertinence to neuromyelitis optica and other demyelinating diseases of the central nervous system. *Neuroscience* 2010, 168: 982–1008.
- Gow A, Southwood CM, Li JS, Pariali M, Riordan GP, Brodie SE, *et al.* CNS myelin and Sertoli cell tight junction strands are absent in *Osp/claudin-11* null mice. *Cell* 1999, 99: 649–659.
- Morita K, Sasaki H, Fujimoto K, Furuse M, Tsukita S. Claudin-11/OSP-based tight junctions of myelin sheaths in brain and Sertoli cells in testis. *J Cell Biol* 1999, 145: 579–588.
- Bhat MA, Rios JC, Lu Y, Garcia-Fresco GP, Ching W, St Martin M, *et al.* Axon-Glia interactions and the domain organization of

- myelinated axons requires neurexin IV/Caspr/Paranodin. *Neuron* 2001, 30: 369–383.
21. Kotini M, Barriga EH, Leslie J, Gentzel M, Rauschenberger V, Schambony A, *et al.* Gap junction protein Connexin-43 is a direct transcriptional regulator of N-cadherin *in vivo*. *Nat Commun* 2018, 9: 3846.
  22. Altevogt BM, Kleopa KA, Postma FR, Scherer SS, Paul DL. Connexin29 is uniquely distributed within myelinating glial cells of the central and peripheral nervous systems. *J Neurosci* 2002, 22: 6458–6470.
  23. Kleopa KA, Orthmann JL, Enriquez A, Paul DL, Scherer SS. Unique distributions of the gap junction proteins connexin29, connexin32, and connexin47 in oligodendrocytes. *Glia* 2004, 47: 346–357.
  24. Norton WT, Poduslo SE. Myelination in rat brain: changes in myelin composition during brain maturation. *J Neurochem* 1973, 21: 759–773.
  25. Nave KA, Werner HB. Myelination of the nervous system: mechanisms and functions. *Annu Rev Cell Dev Biol* 2014, 30: 503–533.
  26. Barnes-Véléz JA, Aksoy Yasar FB, Hu J. Myelin lipid metabolism and its role in myelination and myelin maintenance. *Innov* 2023, 4: 100360.
  27. Poitelon Y, Kopec AM, Belin S. Myelin fat facts: an overview of lipids and fatty acid metabolism. *Cells* 2020, 9: 812.
  28. Quarles RH. Myelin-associated glycoprotein (MAG): past, present and beyond. *J Neurochem* 2007, 100: 1431–1448.
  29. Snaidero N, Velte C, Myllykoski M, Raasakka A, Ignatov A, Werner HB, *et al.* Antagonistic functions of MBP and CNP establish cytosolic channels in CNS myelin. *Cell Rep* 2017, 18: 314–323.
  30. Sima AAF, Pierson CR, Woltjer RL, Hobson GM, Golden JA, Kupsky WJ, *et al.* Neuronal loss in Pelizaeus-Merzbacher disease differs in various mutations of the proteolipid protein 1. *Acta Neuropathol* 2009, 118: 531–539.
  31. Schmitt S, Castelvetti LC, Simons M. Metabolism and functions of lipids in myelin. *Biochim Biophys Acta* 2015, 1851: 999–1005.
  32. Williams SE, Noel M, Lehoux S, Cetinbas M, Xavier RJ, Sadreyev RI, *et al.* Mammalian brain glycoproteins exhibit diminished glycan complexity compared to other tissues. *Nat Commun* 2022, 13: 275.
  33. Cruz TF, Moscarello MA. Identification of the major sites of enzymic glycosylation of myelin basic protein. *Biochim Biophys Acta BBA Gen Subj* 1983, 760: 403–410.
  34. Bercury KK, Macklin WB. Dynamics and mechanisms of CNS myelination. *Dev Cell* 2015, 32: 447–458.
  35. Osso LA, Hughes EG. Dynamics of mature myelin. *Nat Neurosci* 2024, 27: 1449–1461.
  36. de Faria O, Pivonkova H, Varga B, Timmler S, Evans KA, Kárádóttir RT. Periods of synchronized myelin changes shape brain function and plasticity. *Nat Neurosci* 2021, 24: 1508–1521.
  37. Kessaris N, Fogarty M, Iannarelli P, Grist M, Wegner M, Richardson WD. Competing waves of oligodendrocytes in the forebrain and postnatal elimination of an embryonic lineage. *Nat Neurosci* 2006, 9: 173–179.
  38. Richardson WD, Kessaris N, Pringle N. Oligodendrocyte wars. *Nat Rev Neurosci* 2006, 7: 11–18.
  39. Cai J, Qi Y, Hu X, Tan M, Liu Z, Zhang J, *et al.* Generation of oligodendrocyte precursor cells from mouse dorsal spinal cord independent of Nkx6 regulation and Shh signaling. *Neuron* 2005, 45: 41–53.
  40. Wang JQ, Gao MY, Gao R, Zhao KH, Zhang Y, Li X. Oligodendrocyte lineage cells: Advances in development, disease, and heterogeneity. *J Neurochem* 2023, 164: 468–480.
  41. Larsen PH, DaSilva AG, Conant K, Yong VW. Myelin formation during development of the CNS is delayed in matrix metalloproteinase-9 and-12 null mice. *J Neurosci* 2006, 26: 2207–2214.
  42. Duncan ID, Radcliff AB. Inherited and acquired disorders of myelin: The underlying myelin pathology. *Exp Neurol* 2016, 283: 452–475.
  43. Knowles JK, Batra A, Xu H, Monje M. Adaptive and maladaptive myelination in health and disease. *Nat Rev Neurol* 2022, 18: 735–746.
  44. Buyanova IS, Arsalidou M. Cerebral white matter myelination and relations to age, gender, and cognition: a selective review. *Front Hum Neurosci* 2021, 15: 662031.
  45. Nave KA, Sereda MW, Ehrenreich H. Mechanisms of disease: inherited demyelinating neuropathies—from basic to clinical research. *Nat Clin Pract Neurol* 2007, 3: 453–464.
  46. Savaskan NE, Weinmann O, Heimrich B, Eyupoglu IY. High resolution neurochemical gold staining method for myelin in peripheral and central nervous system at the light- and electron-microscopic level. *Cell Tissue Res* 2009, 337: 213–221.
  47. Chen J, Yu Y, Wang S, Shen Y, Tian Y, Rizzello L, *et al.* Nanoscale myelinogenesis image in developing brain *via* super-resolution nanoscopy by near-infrared emissive curcumin-BODIPY derivatives. *J Nanobiotechnology* 2024, 22: 106.
  48. Tsai HH, Macklin WB, Miller RH. Distinct modes of migration position oligodendrocyte precursors for localized cell division in the developing spinal cord. *J Neurosci Res* 2009, 87: 3320–3330.
  49. Zhu Q, Tan Z, Zhao S, Huang H, Zhao X, Hu X, *et al.* Developmental expression and function analysis of protein tyrosine phosphatase receptor type D in oligodendrocyte myelination. *Neuroscience* 2015, 308: 106–114.
  50. Schaeren-Wiemers N, Gerfin-Moser A. A single protocol to detect transcripts of various types and expression levels in neural tissue and cultured cells: *in situ* hybridization using digoxigenin-labelled cRNA probes. *Histochemistry* 1993, 100: 431–440.
  51. Zhang C, Chen Z, Zhang D, Wang X, Qiu M, Tan Z. Role of gltp in maturation of oligodendrocytes under the regulation of Nkx2.2. *Mol Neurobiol* 2023, 60: 4897–4908.
  52. Xu D, Liu A, Wang X, Chen Y, Shen Y, Tan Z, *et al.* Repression of Septin9 and Septin2 suppresses tumor growth of human glioblastoma cells. *Cell Death Dis* 2018, 9: 514.
  53. Pei S, Wang X, Wang X, Huang H, Tao H, Xie B, *et al.* Aberrant nuclear *Lamina* contributes to the malignancy of human gliomas. *J Genet Genomics* 2022, 49: 132–144.
  54. Ryan CB, Choi JS, Al-Ali H, Lee JK. Myelin and non-myelin debris contribute to foamy macrophage formation after spinal cord injury. *Neurobiol Dis* 2022, 163: 105608.
  55. García-García ÓD, Carriel V, Chato-Astrain J. Myelin histology: a key tool in nervous system research. *Neural Regen Res* 2024, 19: 277–281.
  56. Carriel V, Campos A, Alaminos M, Raimondo S, Geuna S. Staining methods for normal and regenerative myelin in the nervous system. *Methods Mol Biol* 2017, 1560: 207–218.
  57. Ineichen BV, Weinmann O, Good N, Plattner PS, Wicki C, Rushing EJ, *et al.* Sudan black: a fast, easy and non-toxic method to assess myelin repair in demyelinating diseases. *Neuropathol Appl Neurobiol* 2017, 43: 242–251.
  58. Teo W, Caprariello AV, Morgan ML, Luchicchi A, Schenk GJ, Joseph JT, *et al.* Nile Red fluorescence spectroscopy reports early physicochemical changes in myelin with high sensitivity. *Proc Natl Acad Sci U S A* 2021, 118: e2016897118.
  59. Swire M, Ffrench-Constant C. Staining and quantitative analysis of myelinating oligodendrocytes in the mouse grey matter. *Bio Protoc* 2020, 10: e3792.
  60. Longair MH, Baker DA, Douglas Armstrong J. Simple neurite tracer: open source software for reconstruction, visualization and analysis of neuronal processes. *Bioinformatics* 2011, 27: 2453–2454.
  61. van Tilborg E, van Kammen CM, de Theije CGM, van Meer MPA, Dijkhuizen RM, Nijboer CH. A quantitative method for



- microstructural analysis of myelinated axons in the injured rodent brain. *Sci Rep* 2017, 7: 16492.
62. Teo W, Morgan ML, Stys PK. Quantitation of the physicochemical properties of myelin using Nile Red fluorescence spectroscopy. *J Neurochem* 2025, 169: e16203.
  63. Huang H, He W, Tang T, Qiu M. Immunological markers for central nervous system *Glia*. *Neurosci Bull* 2023, 39: 379–392.
  64. Wang Y, Sun B, Shibata B, Guo F. Transmission electron microscopic analysis of myelination in the murine central nervous system. *STAR Protoc* 2022, 3: 101304.

**Publisher's Note** Springer Nature remains neutral with regard to jurisdictional claims in published maps and institutional affiliations.

Springer Nature or its licensor (e.g. a society or other partner) holds exclusive rights to this article under a publishing agreement with the author(s) or other rightsholder(s); author self-archiving of the accepted manuscript version of this article is solely governed by the terms of such publishing agreement and applicable law.